Shear-induced migration of a viscous drop in a viscoelastic liquid near a wall at high vis-1 2 cosity ratio: reverse migration 3 Swarnajay Mukherjee<sup>1</sup>, Anik Tarafder<sup>2</sup>, Abhilash Reddy Malipeddi<sup>2</sup> and Kausik Sarkar<sup>2</sup> 4 <sup>1</sup>Department of Mechanical Engineering 5 University of Delaware 6 7 <sup>2</sup>Department of Mechanical and Aerospace Engineering 8 George Washington University 9 10 11 12 Corresponding Author: Kausik Sarkar 13 Department of Mechanical and Aerospace Engineering 14 15 George Washington University 800 22<sup>nd</sup> Street NW, Suite 3000 16 Washington, DC 20052 17 18 Ph: 202-994-2724 19 Email: Sarkar@gwu.edu

1 Abstract

Wall-induced migration of a viscous drop in a viscoelastic fluid subjected to a plane shear is numerically simulated to investigate the effects of drop/matrix viscosity ratio. In a Newtonian system, drop migration away from the wall is inhibited as the viscosity ratio is increased. Here, we show that the introduction of the matrix viscoelasticity further decreases the migration and can even reverse its direction 'from away' to 'towards the wall', a phenomenon not seen in Newtonian systems. The migration towards or away from the wall eventually settles in a quasi-steady state that only depends on the instantaneous wall separation independent of the initial position of the drop. Drops migrating towards the wall initially increase their velocity, but as they approach the wall, they decelerate, showing a non-monotonic variation. The migration direction depends on the viscosity ratio, viscoelasticity (Deborah number), and the capillary number. We compute phase diagrams in the parameter space showing boundaries where migration changes direction. The critical Deborah number (at a fixed viscosity ratio) and the critical viscosity ratio (at a fixed Deborah number) for direction reversal approximately scales with the inverse of the capillary number.

**Keywords**: drop, migration, viscoelastic, FENE, computational, emulsion

### 1. Introduction

1

15

16

17

18

19

20

21

22

23

24

2 The motion of drops and particles plays a critical role in many industrial applications such as food and polymer processing as well as in biological flows [1-4]. It can give rise to an inhomogeneous 3 distribution of fillers in processed polymeric parts [5] and a cell-free layer close to the wall in 4 blood vessels [6-8]. Recent developments in microfluidics have led to renewed interest in particle 5 and cell migration studies where inertia, viscoelasticity, confinement, and particle size individually 6 7 or jointly could influence, and therefore could be manipulated to result in desired paths of suspended particles in the flow channel [9-14]. Although migration of rigid particles in viscoelastic 8 9 medium has received much attention, the literature is extremely meager for viscoelastic effects on drop migration [3]. Drop deformability can introduce lateral migration even in inertialess Newto-10 nian flow [15-17]. Deformability of particles can promote migration away from the wall in both 11 viscous and viscoelastic medium where the latter seemed to reduce migration velocity and the 12 13 migration velocity scales with the inverse square of instantaneous separation from wall [18]. Here, we extend our previous study of a viscosity-matched system to a high viscosity ratio system. 14

Migration of a single particle in simple flow conditions can provide great insight into the physics of fluid suspension and help to design efficient active or passive cell sorting/particle focusing microfluidic devices [19-23]. It is well known that in absence of inertia, reversibility of Stokes flow prevents any lateral motion of a neutrally buoyant rigid sphere in a shear flow near a wall [24-26]. Reversibility is broken by any one of several factors such as particle deformability, viscoelasticity or inertia. Numerous studies have been devoted to the investigation of lateral migration of drops, capsules and particles in shear (see [27] for a review of the literature before 1980). Effects of viscoelasticity on migration, especially for rigid particles, as noted before have also been investigated by various groups [9, 10, 28-34]. However, drop migration in presence of viscoelasticity has received very little attention [31].

- 25 Readers are referred to our previous article [18] for a detailed discussion of the migration literature.
- As noted above, the literature is extremely meager for viscoelastic effects on drop migration. There
- 27 has only been a perturbative study in the limit of small deformation using a second-order fluid
- 28 model [31]; it predicted that drop migration is promoted by both drop and matrix phase viscoelas-

ticity. Viscoelastic effects are often subtle and defy intuition, which is largely formed by our understanding of Newtonian fluid mechanics. The viscoelastic literature is fraught with contradictory findings—e.g. whether viscoelasticity increases or decreases drop deformation in free shear [35-38]—along with no standard viscoelastic constitutive equation. For particle migration, the reasoning advanced is often physical and heuristic as in the case of a sphere in a shear flow between parallel plates, where the difference of the viscoelastic forces on the upper and the lower hemispheres was estimated to cause the lateral migration velocity with a cubic dependence on the blockage ratio of the particle [9, 34]. A similar theory balancing the drag force on a sphere with the viscoelastic force arising from the first normal stress difference varying with the local shear rate was used to explain the viscoelastic focusing seen in a microfluidic experiment with a polyvinyl pyrrolidone solution [11] as well as in a dilute DNA solution [21]. The deformable drop, as we noted before, introduces additional considerations. The situation demands careful analysis of canonical problems such as single drop migration with the simplest possible constitutive equations to help us understand the underlying physics.

The drop migration, we showed, is caused by the velocity induced by a stresslet field created by the drop in presence of the wall [39]. In our previous article, we gave a detailed derivation of the stresslet-induced migration velocity using a Green's function formulation including the viscoelastic contribution [18]. It clearly showed that the migration velocity arises from three different effects—an interfacial contribution, a viscoelastic contribution, and a third contribution arising from non-unity viscosity ratio—the first of the three pushing drops away from the wall and the latter two pulling towards the wall. For the viscosity matched system, in the range of Deborah numbers investigated, although viscoelasticity hindered lateral migration away from the wall, it did not change the migration direction. Here, we lift the restriction on the viscosity ratio. We would show that a high enough ratio of the drop to the matrix viscosity can reverse the migration direction to towards the wall. Also note that for a Newtonian system, BEM simulation [40] showed that the migration velocity of a drop for a high enough viscosity ratio displays a significant deviation from the analytical expressions obtained using a perturbation method [31]. Such considerations amply justify the present study.

- As in [18], we use a front tracking finite difference method and employ a modified version of the
- 2 finitely extensible nonlinear elastic model due to Chilcott and Rallison (FENE-MCR) [41]. The
- 3 model has one relaxation time, a constant shear viscosity and a positive first normal stress differ-
- 4 ence—all characteristics of a Boger fluid—and has been used in many viscoelastic studies [42-46].
- 5 The mathematical formulation and its numerical implementation are described in section 2. Sec-
- 6 tion 3 presents and discusses the results of the simulation, followed by conclusion in section 4.

### 2. Mathematical formulation and numerical implementation

9

8

- 10 The mathematical formulation underlying our computational tool for simulating drops with visco-
- elastic constitutive equations has been described in our recent publication [18]. The complete drop-
- let matrix system is governed by the incompressible momentum conservation equations:

13 
$$\frac{\partial(\rho \mathbf{u})}{\partial t} + \nabla \cdot (\rho \mathbf{u} \mathbf{u}) = \nabla \cdot \mathbf{\tau} - \int_{\partial \mathbf{B}} d\mathbf{x}_{\mathbf{B}} \kappa \mathbf{n} \Gamma \, \delta(\mathbf{x} - \mathbf{x}_{\mathbf{B}}), \tag{1}$$

$$\nabla \cdot \mathbf{u} = 0 \tag{2}$$

- in the entire domain  $\Omega$ . The total stress  $\tau$  is decomposed into pressure, polymeric and viscous
- 16 parts

17 
$$\mathbf{\tau} = -p\mathbf{I} + \mathbf{T}^p + \mathbf{T}^v, \quad \mathbf{T}^v = \mu_s \mathbf{D},$$
 (3)

- where p is the pressure,  $\mu_s$  is the solvent viscosity, and  $\mathbf{D} = (\nabla \mathbf{u}) + (\nabla \mathbf{u})^T$  is the deformation rate
- 19 tensor. The superscript T represents the transpose.  $\mathbf{T}^p$  is the extra stress (or viscoelastic stress) due
- to the presence of polymer. In equation (1)  $\Gamma$  is the interfacial tension (constant),  $\partial B$  represents
- 21 the surface of the drop consisting of points  $\mathbf{x}_B$ ,  $\kappa$  the local curvature,  $\mathbf{n}$  the outward normal, and
- 22  $\delta(\mathbf{x} \mathbf{x}_B)$  is the three-dimensional Dirac delta function. The FENE-CR constitutive equation in
- 23 terms of the conformation tensor A is given by [41] (see a detailed discussion of the method and its
- 24 use in [18]):

25 
$$\frac{\partial \mathbf{A}}{\partial t} + \mathbf{u} \cdot \nabla \mathbf{A} = \nabla \mathbf{u} \cdot \mathbf{A} + \mathbf{A} \cdot (\nabla \mathbf{u})^{T} - \frac{f}{\lambda} (\mathbf{A} - \mathbf{I}) \text{ where } f = \frac{L^{2}}{L^{2} - tr(\mathbf{A})}.$$
 (4)

The relation between the stress  $T^p$  and conformation tensor A is:

$$1 \qquad \mathbf{A} = \left(\frac{\lambda}{\mu_p f}\right) \mathbf{T}^p + \mathbf{I} \ . \tag{5}$$

2 Therefore, the stress constitutive equation becomes:

$$3 \qquad \frac{\partial \mathbf{T}^{p}}{\partial t} + \left\{ \mathbf{u} \cdot \nabla \mathbf{T}^{p} - \nabla \mathbf{u} \cdot \mathbf{T}^{p} - \mathbf{T}^{p} \cdot \nabla \mathbf{u}^{T} \right\} + f \mathbf{T}^{p} \left[ \frac{\partial}{\partial t} \left( \frac{1}{f} \right) + \mathbf{u} \cdot \nabla \left( \frac{1}{f} \right) \right] + \frac{f}{\lambda} \mathbf{T}^{p} = \frac{f}{\lambda} \mu_{p} \mathbf{D}.$$
 (6)

4 where 
$$f = \frac{L^2 + \frac{\lambda}{\mu_p} \left( \sum T_{ii}^p \right)}{L^2 - 3},$$
 (7)

- 5  $\mu_p$  is the polymeric viscosity,  $\lambda$  is the relaxation time, and L is the finite extensibility. FENE-CR
- 6 model introduces finite extensibility limiting the maximum length of the end-to-end vector for the
- 7 polymer molecule. In the limit of  $L \rightarrow \infty$  we obtain the Oldroyd-B equation. The terms
- 8  $f\mathbf{T}^p \left[\frac{\partial}{\partial t} \left(\frac{1}{f}\right) + \mathbf{u} \cdot \nabla \left(\frac{1}{f}\right)\right]$  are negligible in our simulations, and by dropping them we arrive at
- 9 the FENE-MCR equation:

10 
$$\frac{\partial \mathbf{T}^{p}}{\partial t} + \left\{ \mathbf{u} \cdot \nabla \mathbf{T}^{p} - \nabla \mathbf{u} \cdot \mathbf{T}^{p} - \mathbf{T}^{p} \cdot \nabla \mathbf{u}^{T} \right\} + \frac{f}{\lambda} \mathbf{T}^{p} = \frac{f}{\lambda} \mu_{p} \mathbf{D}.$$
 (8)

- By using an elastic and viscous stress splitting method used by [47], the viscoelastic stress can be
- expressed in the following form:

14

17

18

19

13 
$$(\mathbf{T}^{p})^{n+1} = \left[ (\mathbf{T}^{p})^{n} - (\mu_{p}\mathbf{D})^{n} \right] e^{-(f/\lambda)\Delta t} + (\mu_{p}\mathbf{D})^{n} - \frac{\lambda}{f} \left[ \mathbf{u} \cdot \nabla \mathbf{T}^{p} - \nabla \mathbf{u} \cdot \mathbf{T}^{p} - \mathbf{T}^{p} \cdot \nabla \mathbf{u}^{T} \right]^{n} \left[ 1 - e^{-(f/\lambda)\Delta t} \right].$$
 (9)

A spherical drop of radius a is placed in a computational domain at t = 0 in close proximity—

distance  $h_i$ —to the bottom wall (equidistant from the side boundaries) (Fig.1a frame 2). Although

the problem of interest is a simple shear flow near a wall, computationally one needs a finite com-

putational domain of sufficiently large dimensions with conditions imposed on the boundaries to

simulate the shear flow. We choose the size to be  $L_x = 10a$ ,  $L_y = 10a$  and  $L_z = 5a$  in the flow, gra-

dient and the vorticity directions, which was shown to be sufficient in our previous investigations

[15, 18, 48]. The upper plate (y-direction domain boundary) is impulsively started (in the x-direc-

22 tion) with a velocity U and the lower plate is moving with a velocity U at t=0 creating a shear

rate of  $\dot{\gamma} = 2U/L_{v}$ . Periodic conditions are imposed in the flow and the vorticity directions. The

drop is described by a triangulated front distinct from the regular Cartesian grid used to solve the 1 flow field; the front is adaptively regridded to prevent excessive distortion of the front elements. 2 3 A multigrid method is used for the pressure Poisson equation, and an ADI method is used to alleviate the diffusion restriction on the time step. Other details can be found in the previous papers 4 [47, 49-54]. We use  $\alpha$  and  $\dot{\gamma}^{-1}$  for non-dimensionalizing length and time scales respectively (with 5  $t' = t\dot{\gamma}$ ). The dimensionless parameters are Reynolds number  $\text{Re} = \rho_m a^2 \dot{\gamma}/\mu_m$  capillary number 6  $Ca = \mu_m a\dot{\gamma}/\Gamma$ , Deborah number  $De = \lambda\dot{\gamma}$  (which for the present purpose is similar to the Weissen-7 berg number), viscosity ratio  $\lambda_{\mu} = \mu_d/\mu_m$ , density ratio  $\lambda_{\rho} = \rho_d/\rho_m$  and  $\beta = \mu_{pm}/\mu_m$ —the ratio 8 of the polymeric to the total drop viscosity. Additionally, the initial condition is characterized by 9 the nondimensional drop-wall separation  $h_i/a$ . In the matrix, the viscosity is  $\mu_m = \mu_{sm} + \mu_{pm}$ , the 10 sum of the solvent and polymeric viscosities. In all of our simulations, the density ratio has been 11 kept fixed at a value of unity. We have chosen  $\beta = 0.9$  and L = 20. In our previous study of the 12 viscosity matched case, we found that the migration velocity become insensitive to L above this 13 value [18]. Effects of  $\beta$  variation have been investigated in detail for the viscosity-matched sys-14 tem to show that the viscoelastic effects are largely governed by the product  $\beta De$  [18]. The ex-15 plicit nature of the code restricts us (despite the ADI implementation of the viscous terms) to a 16 small non-zero Reynolds number which is kept at a value of 0.03 where inertial effects are negli-17 gible. Effects of the top wall (a numerical artifact) were investigated to find that for h/a < 3.518 dynamics remain independent of the top wall. Convergence of the viscoelastic algorithm used to 19 20 simulate fluids with Oldroyd-B constitutive relation has been established for a number of drop dynamic problems—deformation in shear flows [37, 38, 55], high viscosity ratio system [56], drop 21 retraction [57] and sedimentation in quiescent fluid [58]. For the FENE-MCR relation, grid inde-22 23 pendence was investigated for shear induced drop migration in our previous paper [18]. In this study, we choose 128 x 128 x 64 discretization in the flow, gradient and vorticity directions (the 24 25 effects of discretization is briefly discussed below). We note that in our previous studies [15, 18, 48], we imposed an impulsively started velocity 2U26 on the upper (y-directional) boundary and a zero velocity on the lower one to create the shear flow 27 with the same rate  $\dot{\gamma} = 2U/L_v$  (Figure 1a, frame 1). The two flows (frames 1 and 2) are equivalent 28

under Galilean transformation, and therefore the physics remains the same in both (representing two different reference frames). However, note that numerically the drop shapes and motion are determined by the movement of the mesh points on the front using velocity interpolated from the 3D Cartesian grid, and therefore they are prone to numerical error of the particular discretization level. Such grid related issues resulting in the sensitivity of particle trajectory were also observed in finite element simulations of deformable particles in a channel flow [16], where a particle placed initially at the diagonal of a square cross-section didn't exactly follow the diagonal line of the cross-section during lateral movement. Our choice in favor of the symmetric flow (frame 2 in Figure 1a) is dictated by a numerical investigation of the results in two reference frames (Figure 1). In Figure 1(b), we see that a drop placed at the center of the domain, therefore expected to not move, shows a very small fluctuating initial lateral velocity, due to the drop deformation and initial adjustment. However, eventually, only the flow in symmetric frame 2 leads to a zero velocity preserving the imposed symmetry of the computational flow. The one in the asymmetric frame leads to small but finite positive lateral velocity. For the physical flow of interest here, the computational domain, as noted, is only a numerical artifact, and therefore the centerline is not of any significance. However, such numerical errors are to be avoided if possible. We also investigate a drop in close proximity to the lower boundary and compute the flow in two different reference frames at different discretization levels  $64 \times 64 \times 32$ ,  $128 \times 128 \times 64$  and  $256 \times 256 \times 128$ . In Figure 1(c), the slip velocity (measured relative to the local shear velocity) and deformation (in the inset) plotted for the two reference frames don't differ at the same discretization, both reducing with increased discretization. However, in Figure 1(d), we note that although results in both reference frames eventually converge with increasing discretization, frame 2 converges faster. We therefore choose frame 2 with 128×128×64 discretization.

1

2

3

4

5

6

7

8

9

10

11

12

13

14

15

16

17

18

19

20

21

22

23

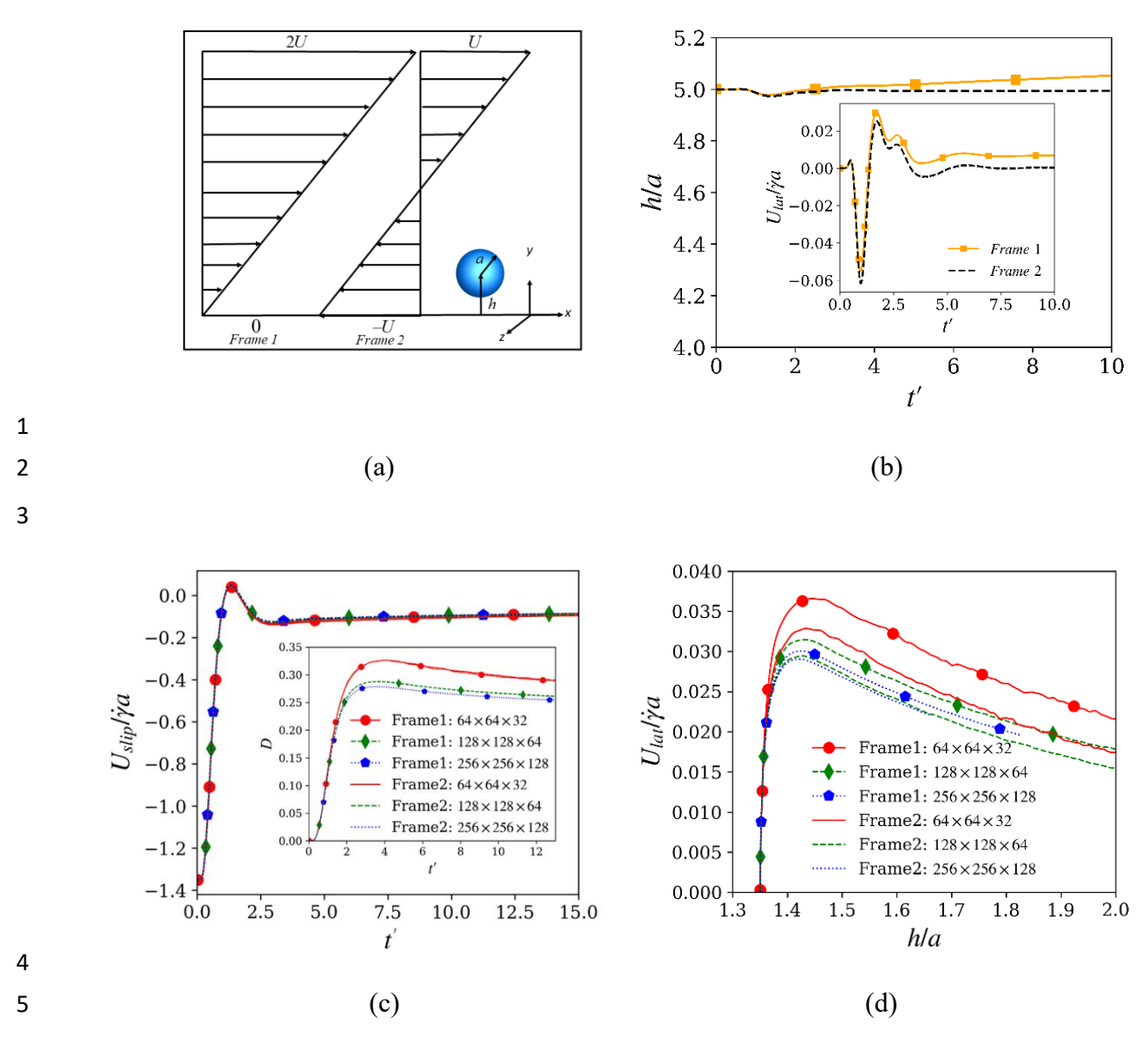


**Figure 1**. (a) Schematic of the problem in two reference frames, (b) Drop position and migration velocity (inset) in two reference frames for Ca=0.2, De=0.5,  $\lambda_{\mu}=10$  (initially placed at the center of the domain ( $h_i/a=5.0$ , equidistance from both the walls). (c) Slip velocity, drop deformation (inset) and (d) migration velocity a viscous drop in a viscoelastic fluid for three grid resolutions in two reference frames for Ca=0.2, De=0.5,  $\lambda_{\mu}=1.0$  and initial position  $h_i/a=1.35$ .

## 3. Results

In our recent study of a viscosity-matched system [18], we developed a theory of drop migration using Stokes Green's function to show that the migration velocity is determined by the image

- stresslet field induced by the drop because of the presence of the wall. Accordingly, far from the
- 2 wall, the migration velocity can be written as

14

15

16

$$3 U_{lat} = -\frac{1}{8\pi\mu_{m}} \left(\frac{9}{8h^{2}}\right) \left(S_{22}^{int} + S_{22}^{vrat} + S_{22}^{NN}\right), (10)$$

where three different stresslet terms are 1) interfacial stresslet  $S_{22}^{\rm int}$  arising from interfacial tension 4 acting at the drop interface, a purely geometric term determined by the drop shape, 2)  $S_{22}^{vrat}$  arising 5 due to non-unity viscosity ratio, and 3)  $S_{22}^{NN}$  arising from viscoelastic stresses around the drop (def-6 initions of the  $S_{22}$ 's are given in [18]). The matrix viscoelasticity affects the migration in two 7 competing ways. It decreases the drop inclination angle thereby increasing the interfacial contri-8 9 bution aiding migration, which however is outweighed by the direct inhibitory effect of the viscoelastic stresses resulting in a net reduction in migration velocity. From the theory, it is clear that 10 the second term due to the viscosity ratio also inhibits migration at large viscosity ratios. Here, we 11 investigate this effect of the viscosity ratio. Due to the rather small drop-wall distances considered 12

here, the stresslet-based theory developed in [18] is not valid and therefore cannot be used for

quantitative comparison. However, it helps us understand the results.

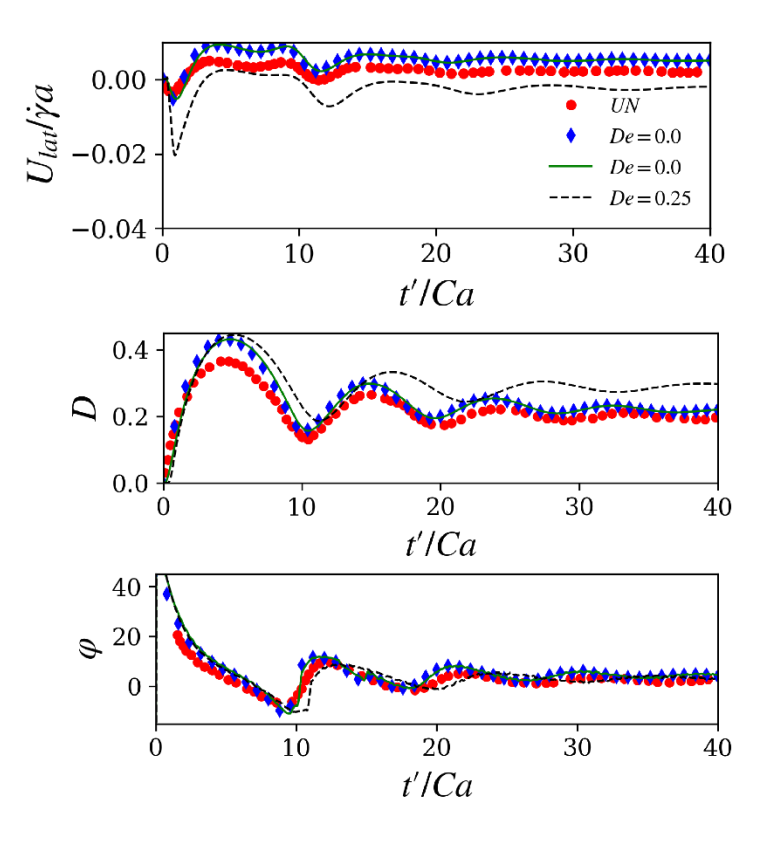


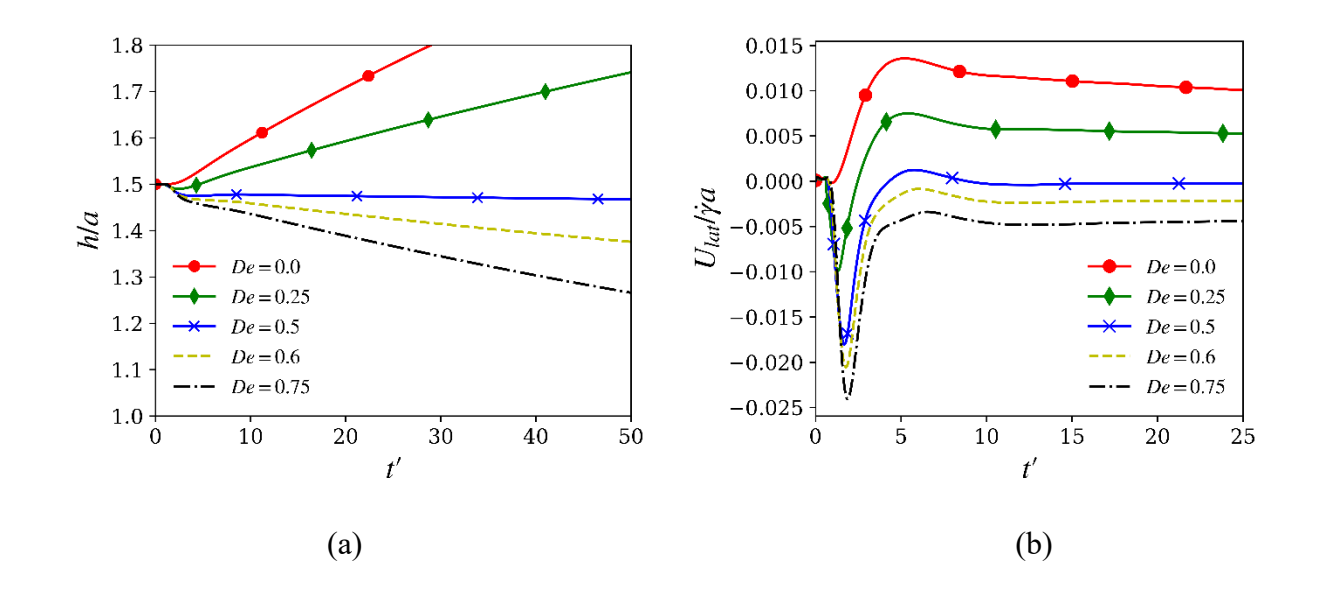
**Figure 2**. Lateral velocity, deformation and orientation angle for Ca = 1.5,  $\lambda_{\mu} = 10$ , and  $h_i/a = 1.5$  are compared with BEM simulations of Uijttewaaal and Nijhof (UN). Dotted curves in color blue (our simulation) and red (BEM) are computed with initially fully developed shear for the viscous case (De = 0). The other two curves are with impulsively started flow for De = 0 (solid) and De = 0.25 (dash).

### 3.1. Comparison with BEM solution and effects of Deborah number

In our previous paper [18], we showed a very good comparison between our results—drop deformation and migration velocity for the Newtonian system of a viscosity matched drop in a wall-bounded shear—with those from BEM simulations [59] and theoretical expressions of Chan and Leal [31] and Shapira and Haber [60]. In Fig.2 we consider the case of a high viscosity ratio of  $\lambda_{\mu} = 10$  at Ca = 1.5 and  $h_{\nu}/a = 1.5$ . We first consider a Newtonian case (De = 0) and compare the time evolution of lateral velocity, deformation and orientation angle with BEM simulation [40]. We use time nondimensionalization  $t'/Ca = t\Gamma/\mu_{m}a$  of the BEM article. The deformation shows oscillations and wobbly motion as is typical for high viscosity ratio drops. The inclination angle oscillates, but eventually decreases away from the extension axis of the shear at  $\pi/4$  to align with

the flow. The deformation and the inclination angle show excellent match between the two independent computations except at the initial period. The small discrepancy (between the blue and the red dotted curved) is due to the finite inertia (Re = 0.03) in our computation. However, they all show the same details of time-variation (magnitude and periodicity) albeit with slight variation in magnitudes, especially for the velocity. Note that unlike in BEM computation of Stokes flow, due to the finite inertia in our computation, it takes a finite time for the shear to establish after the impulsive start of the top boundary. For comparison with the BEM simulation, we have used a fully developed linear shear flow as the initial velocity field as opposed to fluid initially at rest impulsively started by the top and the bottom boundaries as in all other computations in the paper.

In the same figure, we include a viscoelastic case—De=0.25. Viscoelasticity increases deformation, changes inclination, and retards migration velocity. For De=0.25, the velocity is negative and the drop moves towards the wall. Both higher viscosity ratio and viscoelasticity retard migration, but in combination, they here reverse the direction of migration. For the viscosity matched cases, within the range of Deborah numbers considered [18], we did not observe such a reversal. However, rigid spheres—which is retrieved for a drop in the limit of  $\lambda_{\mu} \rightarrow \infty$ —were shown to migrate towards the closest wall in a shear flow [61].



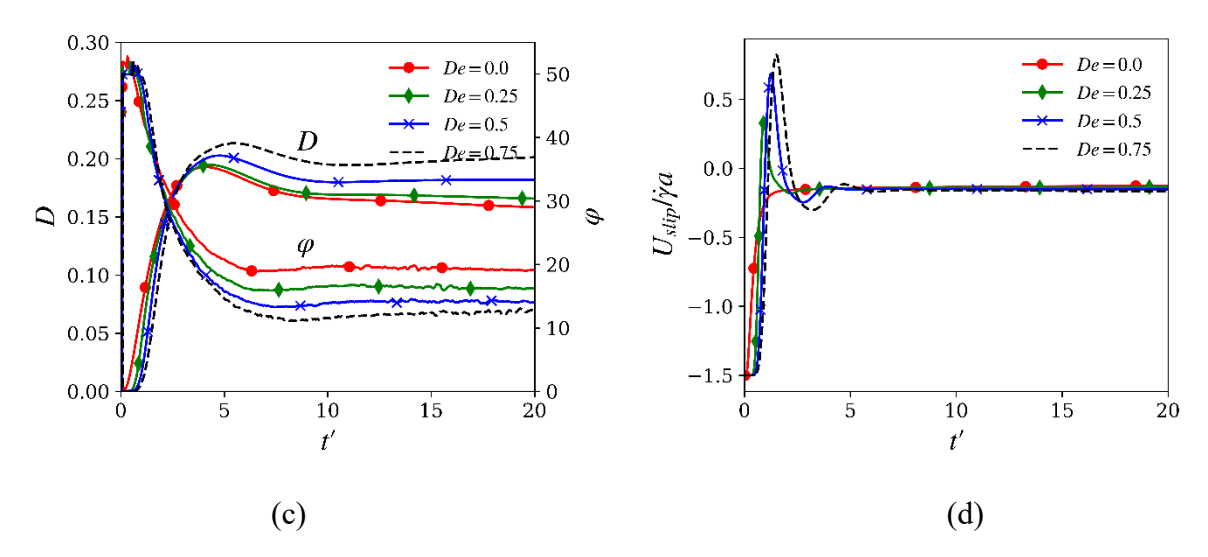


**Figure 3**. Drop migration for varying De for Ca = 0.2,  $\lambda_{\mu} = 10$  and  $h_i/a = 1.5$ : (a) Drop height, (b) lateral migration velocity, (c) deformation and inclination angle, and (d) slip velocity with nondimensional time.

3

4

5 6

7

8

9

10

11

12

13

14

15

16

17

18

19

20

21

22

In Fig. 3(a), we plot the evolution of the dimensionless distance of the drop from the wall for varying De at Ca = 0.2,  $\lambda_u = 10$ , and  $h_i / a = 1.5$ . With increasing viscoelasticity, the migration away from the wall gets retarded, and eventually reverses its direction to towards the wall at De= 0.5. Fig. 3(b) shows the same by plotting the migration velocity as a function of time. With increasing De, the drop is pulled more towards the wall. When the viscoelastic contribution can overcome the combined effect of interfacial and viscous stresses, the drop migrates towards the wall. Fig. 3(c) plots drop deformation and the angle of inclination as a function of time for different De with other parameters kept the same. The deformation increases with increasing viscoelasticity due to viscoelastic stretching as well as the drop being nearer to the wall experiences a higher local strain rate. Previous numerical studies described the importance of inclination angle in migration [40]. At this high  $\lambda_{\mu}=10$  , the inclination angle even for a Newtonian case is quite small,  $19^{0}$ . The decrease in angle with increasing Deborah number considered here is not too large (120~160). Slip velocities (Fig. 3d) show that during the transient phase, there is an overshoot and for higher De, the value can become positive i.e., the drop leads the flow. This is only temporary, and a quasisteady state is reached where slip velocities are negative and do not vary significantly with Deborah number. The drop deformation is computed from the farthest and the nearest points on the drop

interface, which in turn is evolved by velocities interpolated on the front vertices from the field in the Eulerian grid. This numerical procedure gives rise to the slight lack of smoothness seen in some of the curves in Figure 3(c) and in other figures below.

In Fig. 4, we investigate lateral migration as a function of separation from the wall with drops initially placed at different initial heights from the wall. Three cases, De = 0, 0.25 and 0.75 are considered. As we saw in the viscosity matched system, the curves for different initial heights eventually collapse on each other indicating quasi-steady dynamics independent of the initial condition. For the Newtonian and the De = 0.25 cases, the quasi-steady velocities are positive. However, for De = 0.75, the drop has a negative velocity. For the latter case, as the drop approaches the wall, around h/a = 1.1, the velocity almost reaches zero. The transients are different in the three cases. For the Newtonian and De = 0.25, the velocity initially increases and then settles down as the quasi-steady state is reached. For De = 0.75, the curve looks similar except that the velocity, as mentioned, remains negative.

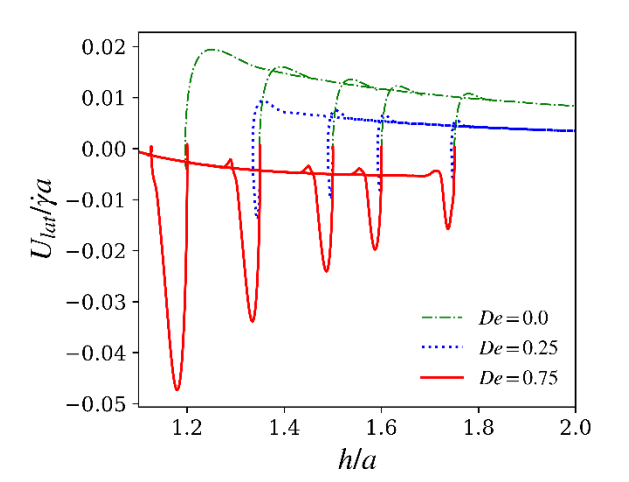


**Figure 4.** Lateral migration velocity as a function of the distance from the wall for Newtonian and viscoelastic cases for Ca = 0.2,  $\lambda_u = 10$  and varying De.

# 3.2. Effects of viscosity ratio and capillary number

Increasing the viscosity ratio  $\lambda_{\mu}$  has two well-known effects on the drop geometry—the deformation decreases and the drop gets increasingly aligned with the flow. In Fig. 5(a), we plot the

- evolution of drop height for Ca = 0.2, De = 0.75 and  $h_i / a = 1.5$  with varying viscosity ratios. The
- drop initially experiences a negative migration velocity for all  $\lambda_{\mu}$  (seen clearly in the inset) moving
- 3 towards the wall but later they settle either for migration away from the wall for  $\lambda_{\mu} < 6.0$ , or to-
- 4 wards the wall for larger  $\lambda_{\mu}$ >6.0. Fig. 5(b) shows very little effects of viscosity ratio on slip ve-
- 5 locity evolution.

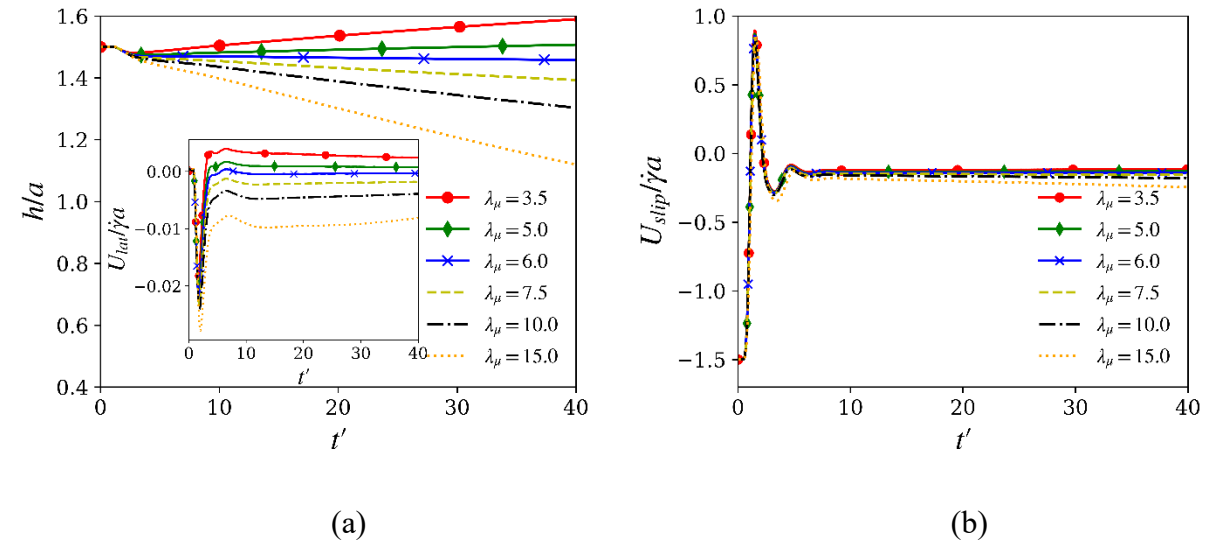
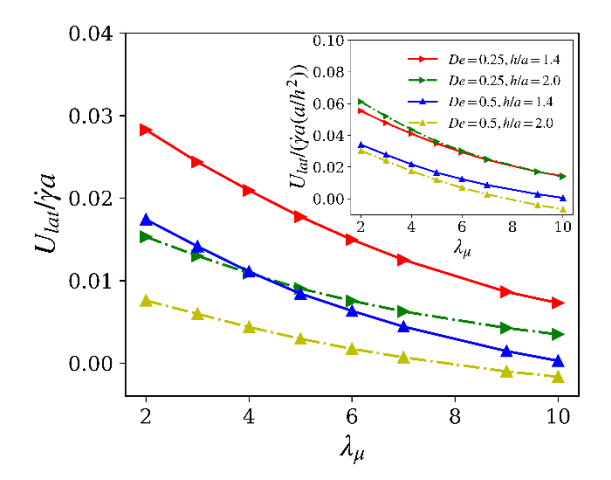


**Figure 5**. (a) Non-dimensional height vs. time for Ca = 0.2, De = 0.75, and  $h_i/a = 1.5$ . The inset shows the time variation of lateral velocity. (b) Time evolution of slip velocity for the same parameters.



7

8

9

Figure 6. Quasi-steady migration velocity as a function of viscosity ratio, at two different Deborah

numbers and h/a (legends are same as in the inset) for Ca = 0.2. Inset shows the same scaled by

 $(a/h)^2$ .

4

7

8

9

10

12

2

Fig. 6 plots the lateral velocity as a function of  $\lambda_{\mu}$  (in the quasi-steady state) for Ca=0.2 and two

6 Deborah numbers. For a particular height, the curves for two *De* are almost parallel to each other.

Given the analytical theory [18, 31] that predicts  $U_{lat}/\dot{\gamma}a \sim Ca(a/h)^2$ , in the inset we plot

 $U_{lat}(h/a)^2/\dot{\gamma}a$  to show that the scaling is only approximate (as was also seen in the viscosity

matched system [18]). For a Newtonian case, Uijttewaaal and Nijhof [40] also observed that the

scaling does not hold exactly except at small  $Ca \sim 0.1$  and large wall separation  $h/a \sim 20$ . In-

11 creasing capillary number increases drop deformation promoting migration away from the wall.

Increasing matrix viscoelasticity pushes the drop towards the wall reducing the validity of the

13 scaling law.

14 15

16

18

19

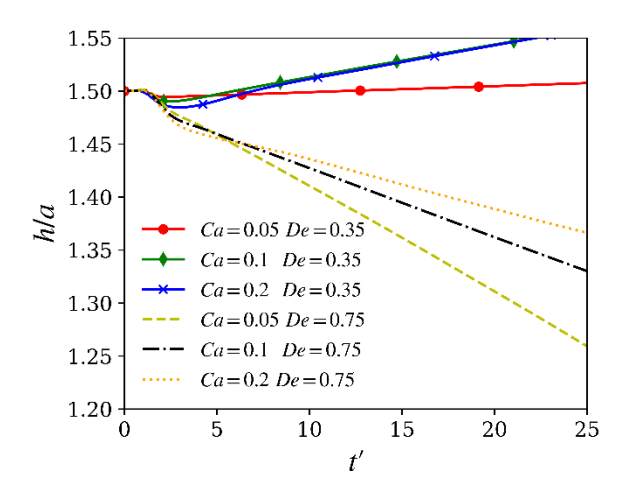
In Fig. 7, we plot the time evolution of drop heights for three different capillary numbers and two

Deborah numbers at  $\lambda_{\mu} = 10$ . At the lower Deborah number De = 0.35, the drop migrates away

from the wall for Ca = 0.2, Ca = 0.1 and Ca = 0.05, migration speed decreasing with decreasing

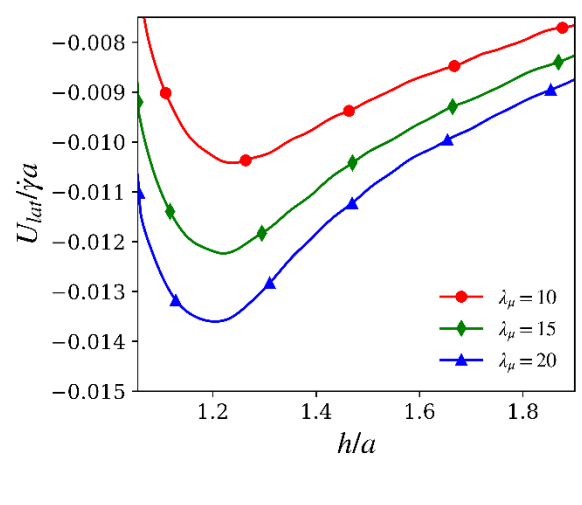
Ca. At De = 0.75, the drop migrates towards the wall for all three Ca values, the absolute speed

of migration increasing with decreasing Ca.

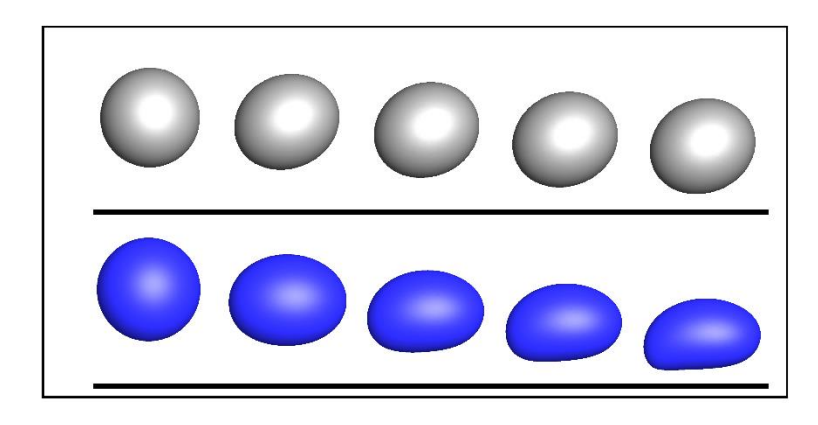


- Figure 7. Evolution of the non-dimensional drop height for different capillary and Deborah num-
- 2 bers and  $\lambda_{\mu} = 10$ .

Fig. 8(a) plots migration velocity for Ca = 0.05, De = 0.75 and varying viscosity ratios, where the drop migrates towards the wall. As the drop approaches the wall, the absolute value of the velocity first increases, reaches a maximum, and then decreases. The maximum velocity magnitude increases with increasing viscosity ratio, with the location shifting slightly towards the wall. The velocity maximum can be explained by noting the following fact. The presence of the wall is the cause of drop migration; far away from the wall the wall-ward migration velocity is small and increases as the drop approaches the wall. However, the motion is finally impeded close to the wall, and the migration velocity has to eventually decrease to zero. Therefore, in its approach to the wall, the absolute velocity would pass through a maximum. The curves have been averaged to eliminate slight oscillations arising due to the numerical issues noted while describing Figure 3(c) further aggravated by the numerical differentiation of the position to compute the velocity. At proximity to the wall, the drop shape is affected by the wall, lubrication forces in the small gap are strong, and the drop experiences strong deformation. Figs. 8(b) shows drop shapes and heights (but not correct x positions) at some consecutive times for two different viscosity ratios. The drop assumes flattened shapes effectively lowering the height of its center of mass.



19 (a)



2 (b)

De = 0.75, Ca = 0.2,  $h_i/a = 1.5$ ,  $\lambda_{\mu} = 20$  (bottom).

Figure 8. (a) Quasi-steady velocities plotted vs. drop height for Ca = 0.05 and De = 0.75 for different viscosity ratios. (b) Shapes of drops (horizontal position is arbitrary) migrating towards the wall (black line) at successive time instants for De = 0.75, Ca = 0.05,  $h_i/a = 1.5$ ,  $\lambda_{\mu} = 10$  (top) and

In Fig. 9, we plot the migration velocity as a function of capillary number at an instantaneous height h/a=1.4 for different De values. With increasing Ca, migration velocity initially increases, reaches a maximum and then slightly reduces. Note that the previous BEM simulation [40] also showed such nonmonotonicity at high viscosity ratios. The deviation from the analytic result  $U_{lat}/\dot{\gamma}a \sim Ca(a/h)^2$  can be seen clearly in the inset where the migration velocity divided by capillary numbers is plotted. The viscoelastic curves follow a similar trend with velocity decreasing and eventually becoming negative with increasing De.

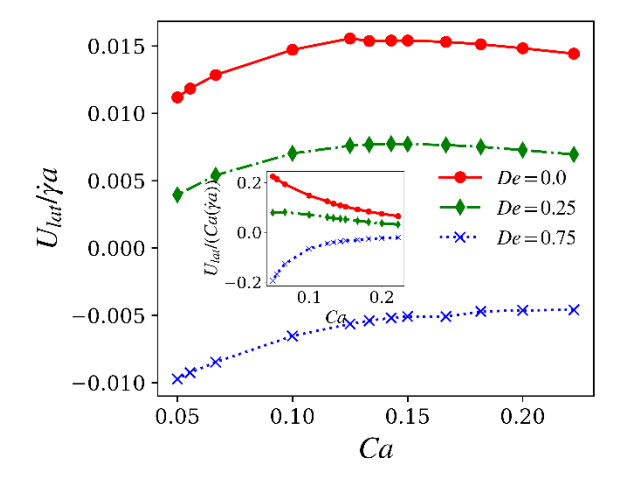


**Figure 9.** Lateral migration velocities plotted for  $\lambda_{\mu} = 10$  and at instantaneous height of 1.4*a* to show Capillary variation of lateral velocities for different Deborah numbers. Inset shows the lateral velocities divided by Ca.

## 3.3. Phase diagrams for positive and negative migration

We have found that increasing viscoelasticity and viscosity ratio promotes migration towards the wall, whereas increasing capillary number pushes it away from the wall. The competition governs the dynamics and results in either a positive or a negative migration velocity for the drop. In this section, we present phase diagrams determining the regions in this parameter space for these two behaviors. Fig. 10(a) plots the phase diagram for Ca and  $\lambda_{\mu}$  for drops initially positioned at  $h_i/a=1.5$  and De=0.75. Each symbol represents a simulation; upward triangles represent drops eventually going away from the wall and downward triangles represent moving towards the wall. As Ca is increased, a higher value of viscosity ratio is required to make the drop migrate down towards the wall. The color contour shows the migration velocity positive i.e., away from the wall for more deformable drops and low viscosity ratios, reducing velocity as viscosity ratio  $\lambda_{\mu}$  is increased and Ca decreased, eventually reversing direction towards the wall. An approximate linear relation  $\lambda_{\mu,critical} \sim Ca^{-1}$  is noticed between the inverse of capillary number and the viscosity ratio. Fig. 10(b) plots a similar phase diagram in De-Ca space for  $h_i/a=1.5$  and  $\lambda_{\mu}=10$ . The drops above the green line (downward triangles) eventually migrate towards the wall, and those below (upward triangles) migrate away from the wall, showing here also an approximately linear relation

- $De_{critical} \sim Ca^{-1}$ . In both figures, away from the phase boundaries the velocity magnitudes increase.
- 2 Note that the stresslet theory and the phenomenological relation for migration both predicted
- $U_{lat}/\dot{\gamma}a \sim (K_1Ca K_2De K_3CaDe)$  [18]. Neglecting the third term for small Ca gives
- $De_{critical} \sim Ca^{-1}$  for zero migration velocity.

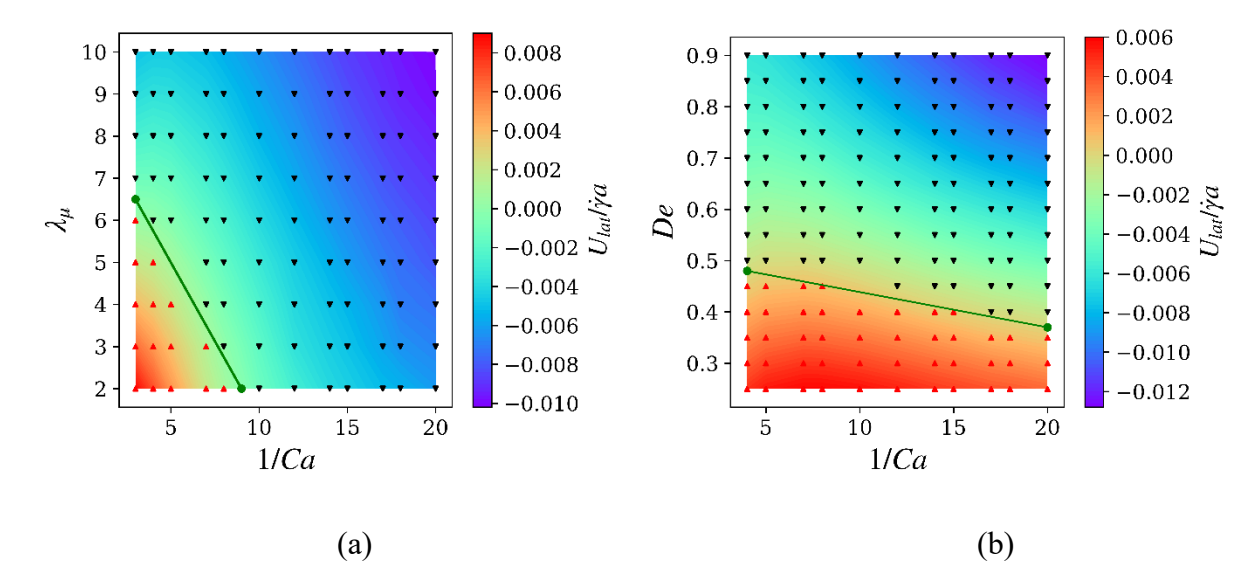


**Figure 10**. Phase diagrams for the direction of drop migration: (a) In  $\lambda_{\mu}$ -Ca space for De = 0.75 and  $h_i/a = 1.5$ . (b) In De-Ca space for  $\lambda_{\mu} = 10$ ,  $h_i/a = 1.5$ . Drops below the green lines migrate away from the wall and those above migrate towards the wall. The color contour describes the migration velocity.

### 4. Conclusions

Following our recent numerical investigation of the migration of a viscosity-matched viscous drop in a viscoelastic matrix [18], in this paper, we investigate the same phenomenon for high drop to matrix viscosity ratios. Our earlier investigation showed that matrix viscoelasticity retards migration of a drop away from the wall—the effect stemming from the viscoelastic normal stresses along the curved streamlines around the drop. Here, we see that at high viscosity ratios, strong enough viscoelasticity can reverse the migration direction from away from the wall to towards the wall. The migration velocity eventually becomes quasi-steady depending only on its instantaneous separation from the wall. For drops migrating towards the wall, their approach velocity shows a non-

- 1 monotonic variation with the distance from the wall. The slip velocity is briefly investigated to
- 2 show that it is not a strong function of  $\lambda_{\mu}$ .

- 4 We noted in our previous work, that the migration is caused by three distinct effects—an interfacial
- 5 term, a viscosity ratio term and a viscoelastic term, the latter two inhibiting the migration away
- 6 from the wall caused by the first one. The competition between the three determines the direction
- of the migration. With numerous simulations varying De, Ca and  $\lambda_{\mu}$ , we obtain phase diagrams
- 8 showing the critical values of parameters that distinguish migration direction towards or away
- 9 from the wall. The critical parameters show approximate relations:  $\lambda_{\mu,critical} \sim Ca^{-1}$  for a fixed De,
- and  $De_{critical} \sim Ca^{-1}$  for a fixed  $\lambda_{\mu}$ . Note that in an emulsion with multiple drops, migration along
- with shear-driven collision determines the final drop distribution—a phenomenon that has been
- studied for Newtonian systems [62, 63]. The wall-ward migration presented here indicates funda-
- mentally different physics for viscoelastic emulsions and warrants further investigation.

14 15

## Acknowledgment

- 16 KS acknowledges partial financial support from NSF Grants No. CBET-0625599, CBET-0651912,
- 17 CBET-1033256, DMR-1239105, CBET-1205322, and CMMI 2019507. Authors acknowledge
- time on the Pegasus cluster at GWU. KS thanks Professor Bill Schowalter for reading a draft and
- offering his insights. The computation was also performed using the Comet cluster at the San
- 20 Diego Supercomputer Center, through the Extreme Science and Engineering Discovery Environ-
- 21 ment (XSEDE) program [64], which is supported by the National Science Foundation grant num-
- 22 ber ACI-1548562 (CTS180042).

### 1 References:

- 2 1. Barbati, A.C., et al., *Complex fluids and hydraulic fracturing*. Annual review of chemical and biomolecular engineering, 2016. 7: p. 415-453.
- 4 2. Morris, J.F., *Toward a fluid mechanics of suspensions*. Physical Review Fluids, 2020. 5(11): p. 110519.
- Raffiee, A.H., S. Dabiri, and A.M. Ardekani, Suspension of deformable particles in Newtonian and viscoelastic fluids in a microchannel. Microfluidics and Nanofluidics, 2019. **23**(2): p. 22.
- 9 4. Shaqfeh, E.S., *On the rheology of particle suspensions in viscoelastic fluids*. AIChE Journal, 2019. **65**(5): p. e16575.
- Hegler, R.P. and G. Mennig, Phase-Separation Effects in Processing of Glass-Bead Filled and Glass-Fiber-Filled Thermoplastics by Injection-Molding. Polymer
   Engineering and Science, 1985. 25(7): p. 395-405.
- Barbee, J.H. and G.R. Cokelet, *The fahraeus effect*. Microvascular research, 1971. 3(1):
   p. 6-16.
- 7. Fåhraeus, R., The suspension stability of the blood. Physiological reviews, 1929. 9(2): p. 241-274.
- 18 8. Tangelder, G.J., et al., *Distribution of blood platelets flowing in arterioles*. American Journal of Physiology-Heart and Circulatory Physiology, 1985. **248**(3): p. H318-H323.
- D'Avino, G., F. Greco, and P.L. Maffettone, Particle migration due to viscoelasticity of the suspending liquid and its relevance in microfluidic devices. Annual Review of Fluid Mechanics, 2017. 49: p. 341-360.
- Zhou, J. and I. Papautsky, *Viscoelastic microfluidics: progress and challenges*.
   Microsystems & Nanoengineering, 2020. 6(1): p. 1-24.
- Leshansky, A.M., et al., *Tunable Nonlinear Viscoelastic `Focusing'' in a Microfluidic Device*. Physical Review Letters, 2007. 98(23): p. 234501.
- Lim, E.J., et al., *Inertio-elastic focusing of bioparticles in microchannels at high throughput*. Nature Communications, 2014. 5(1): p. 4120.
- 29 13. Sarkar, K. and R.K. Singh, *Spatial ordering due to hydrodynamic interactions between a pair of colliding drops in a confined shear*. Physics of Fluids, 2013. **25**(5).
- 31 14. Singha, S., et al., Mechanisms of spontaneous chain formation and subsequent 32 microstructural evolution in shear-driven strongly confined drop monolayers. Soft 33 Matter, 2019. **15**(24): p. 4873-4889.
- Singh, R.K., X.Y. Li, and K. Sarkar, *Lateral migration of a capsule in plane shear near a wall.* Journal of Fluid Mechanics, 2014. 739: p. 421-443.
- Villone, M.M., Lateral migration of deformable particles in microfluidic channel flow of
   Newtonian and viscoelastic media: a computational study. Microfluidics and
   Nanofluidics, 2019. 23(3): p. 1-13.
- Villone, M.M., et al., Numerical simulations of deformable particle lateral migration in tube flow of Newtonian and viscoelastic media. Journal of Non-Newtonian Fluid Mechanics, 2016. **234**: p. 105-113.
- Mukherjee, S. and K. Sarkar, Effects of matrix viscoelasticity on the lateral migration of a deformable drop in a wall-bounded shear. Journal of Fluid Mechanics, 2013. 727: p. 318-345.

- 1 19. Bhagat, A.A.S., S.S. Kuntaegowdanahalli, and I. Papautsky, *Inertial microfluidics for*
- continuous particle filtration and extraction. Microfluidics and Nanofluidics, 2009. 7(2):
   p. 217-226.
- 4 20. Inglis, D.W., et al., *Critical particle size for fractionation by deterministic lateral displacement.* Lab on a Chip, 2006. **6**(5): p. 655-658.
- 6 21. Kang, K., et al., *DNA-based highly tunable particle focuser*. Nature Communications, 2013. **4**(1): p. 2567.
- Yang, S., et al., *Sheathless elasto-inertial particle focusing and continuous separation in a straight rectangular microchannel.* Lab on a Chip, 2011. **11**(2): p. 266-273.
- 10 23. Nieuwstadt, H.A., et al., *Microfluidic particle sorting utilizing inertial lift force*. Biomedical Microdevices, 2011. **13**(1): p. 97-105.
- 24. Saffman, P.G., On the motion of small spheroidal particles in a viscous liquid. Journal of Fluid Mechanics, 1956. 1(05): p. 540-553.
- 14 25. Bretherton, F.P., *The Motion of Rigid Particles in a Shear Flow at Low Reynolds*15 *Number*. Journal of Fluid Mechanics, 1962. **14**(2): p. 284-304.
- Leal, L.G., Advanced Transport Phenomena: Fluid Mechanics and Convective Transport
   2007, New York:: Cambridge University Press.
- Leal, L.G., Particle Motions in a Viscous Fluid. Annual Review of Fluid Mechanics,
   1980. 12(1): p. 435-476.
- 28. Karnis, A. and S.G. Mason, *Particle Motions in Sheared Suspensions. XIX. Viscoelastic Media.* Transactions of the Society of Rheology, 1966. 10(2): p. 571-592.
- 29. Bartram, E., Goldsmith.H.L., and S.G. Mason, *Particle motions in non-newtonian media III. Further observations in elasticoviscous fluids*. Rhelogical Acta, 1975. **14**(9): p. 776-782.
- 30. Ho, B.P. and L.G. Leal, Migration of Rigid Spheres in a 2-Dimensional Unidirectional
   Shear-Flow of a 2nd-Order Fluid. Journal of Fluid Mechanics, 1976. 76(Aug25): p. 783-799.
- 28 31. Chan, P.C.H. and L.G. Leal, *The motion of a deformable drop in a second-order fluid.*29 Journal of Fluid Mechanics, 1979. **92**(01): p. 131-170.
- Feng, J. and D.D. Joseph, *The motion of solid particles suspended in viscoelastic liquids under torsional shear*. Journal of Fluid Mechanics, 1996. **324**: p. 199-222.
- Huang, P.Y., et al., *Direct simulation of the motion of solid particles in Couette and Poiseuille flows of viscoelastic fluids*. Journal of Fluid Mechanics, 1997. **343**: p. 73-94.
- 34. D'Avino, G., et al., *Viscoelasticity-induced migration of a rigid sphere in confined shear flow.* Journal of Non-Newtonian Fluid Mechanics, 2010. **165**(9-10): p. 466.
- 36 35. Tavgac, T., Ph.D thesis (Chemical Engineering), Univ. of Houston, Texas 1972.
- 36. Elmendorp, J.J., Maalcke, R. J., *A study on polymer blending microrheology. 1.* Polymer Engng Sci., 1985. **25**: p. 1041–1047.
- Aggarwal, N. and K. Sarkar, Deformation and breakup of a viscoelastic drop in a
   Newtonian matrix under steady shear. Journal of Fluid Mechanics, 2007. 584: p. 1-21.
- 41 38. Aggarwal, N. and K. Sarkar, *Effects of matrix viscoelasticity on viscous and viscoelastic drop deformation in a shear flow.* Journal of Fluid Mechanics, 2008. **601**: p. 63-84.
- Smart, J.R. and D.T. Leighton, Jr., *Measurement of the drift of a droplet due to the presence of a plane.* Physics of Fluids A: Fluid Dynamics, 1991. **3**(1): p. 21-28.
- 40. Uijttewaal , W.S.J. and E.J. Nijhof *The motion of a droplet subjected to linear shear flow including the presence of a plane wall.* Journal of Fluid Mechanics, 1995. 302: p. 45-63.

- 1 41. Chilcott, M.D. and J.M. Rallison, *Creeping flow of dilute polymer solutions past* cylinders and spheres. Journal of Non-Newtonian Fluid Mechanics, 1988. **29**: p. 381.
- 3 42. Matos, H.M., M.A. Alves, and P.J. Oliveira, *New Formulation for Stress Calculation:*
- *Application to Viscoelastic Flow in a T-Junction*. Numerical Heat Transfer, Part B: Fundamentals, 2009. **56**(5): p. 351.
- Rocha, G.N., R.J. Poole, and P.J. Oliveira, *Bifurcation phenomena in viscoelastic flows through a symmetric 1:4 expansion*. Journal of Non-Newtonian Fluid Mechanics, 2007. **141**(1): p. 1.
- 9 44. Oliveira, P.J. and A.l.I.P. Miranda, *A numerical study of steady and unsteady viscoelastic flow past bounded cylinders*. Journal of Non-Newtonian Fluid Mechanics, 2005. **127**(1): p. 51.
- Sahin, M. and R.G. Owens, On the effects of viscoelasticity on two-dimensional vortex dynamics in the cylinder wake. Journal of Non-Newtonian Fluid Mechanics, 2004.
   123(2–3): p. 121.
- 46. Coates, P.J., R.C. Armstrong, and R.A. Brown, Calculation of steady-state viscoelastic flow through axisymmetric contractions with the EEME formulation. Journal of Non-Newtonian Fluid Mechanics, 1992. 42(1–2): p. 141.
- 18 47. Sarkar, K. and W.R. Schowalter, *Deformation of a two-dimensional viscoelastic drop at*19 non-zero Reynolds number in time-periodic extensional flows. Journal of Non-Newtonian
  20 Fluid Mechanics, 2000. **95**(2-3): p. 315-342.
- Mukherjee, S. and K. Sarkar, *Lateral migration of a viscoelastic drop in a Newtonian* fluid in a shear flow near a wall. Physics of Fluids, 2014. **26**: p. 103102.
- Sarkar, K. and W.R. Schowalter, Deformation of a two-dimensional drop at non-zero
   Reynolds number in time-periodic extensional flows: numerical simulation. Journal of
   Fluid Mechanics, 2001. 436: p. 177-206.
- 50. Li, X.Y. and K. Sarkar, *Drop deformation and breakup in a vortex at finite inertia*.
   Journal of Fluid Mechanics, 2006. 564: p. 1-23.
- 28 51. Li, X. and K. Sarkar, *Drop dynamics in an oscillating extensional flow at finite Reynolds numbers*. Physics of fluids, 2005. **17**(2): p. 027103.
- 52. Li, X.Y. and K. Sarkar, Numerical investigation of the rheology of a dilute emulsion of drops in an oscillating extensional flow. Journal of Non-Newtonian Fluid Mechanics, 2005. 128(2-3): p. 71-82.
- Olapade, P.O., R.K. Singh, and K. Sarkar, *Pairwise interactions between deformable drops in free shear at finite inertia.* Physics of Fluids, 2009. **21**(6): p. 063302.
- Singh, R.K. and K. Sarkar, *Inertial effects on the dynamics, streamline topology and interfacial stresses due to a drop in shear*. Journal of Fluid Mechanics, 2011. 683: p. 149-171.
- 38 55. Aggarwal, N. and K. Sarkar, *Rheology of an emulsion of viscoelastic drops in steady shear.* Journal of Non-Newtonian Fluid Mechanics, 2008. **150**(1): p. 19-31.
- Mukherjee, S. and K. Sarkar, *Effects of viscosity ratio on deformation of a viscoelastic* drop in a Newtonian matrix under steady shear. Journal of Non-Newtonian Fluid Mechanics, 2009. **160**(2-3): p. 104-112.
- Mukherjee, S. and K. Sarkar, *Effects of viscoelasticity on the retraction of a sheared drop.* Journal of Non-Newtonian Fluid Mechanics, 2010. **165**(7-8): p. 340-349.
- Mukherjee, S. and K. Sarkar, *Viscoelastic drop falling through a viscous medium*.
   Physics of Fluids, 2011. 23(1): p. 013101.

- Uijttewaal, W.S.J., E.J. Nijhof, and R.M. Heethaar, *Droplet Migration, Deformation, and Orientation in the Presence of a Plane Wall a Numerical Study Compared with Analytical Theories.* Physics of Fluids a-Fluid Dynamics, 1993. 5(4): p. 819-825.
- Shapira, M. and S. Haber, *Low Reynolds number motion of a droplet in shear flow including wall effects.* International Journal of Multiphase Flow, 1990. **16**(2): p. 305.
- 6 61. Lormand, B.M. and R.J. Phillips, *Sphere migration in oscillatory Couette flow of a viscoelastic fluid.* Journal of Rheology, 2004. **48**(3): p. 551-570.
- Hudson, S.D., Wall migration and shear-induced diffusion of fluid droplets in emulsions.
   Physics of Fluids, 2003. 15(5): p. 1106-1113.
- 10 63. King, M.R. and D.T. Leighton, *Measurement of shear-induced dispersion in a dilute emulsion*. Physics of Fluids, 2001. **13**(2): p. 397-406.
- 12 64. Towns, J., et al., *XSEDE: Accelerating Scientific Discovery*. Computing in Science \& Engineering, 2014. **16**(5): p. 62-74.

- 1 Figure Captions
- 2 Figure 1. (a) Schematic of the problem in two reference frames, (b) Drop position and migration
- velocity (inset) in two reference frames for Ca=0.2, De=0.5,  $\lambda_u=10$  (initially placed at the center
- of the domain ( $h_i/a=5.0$ , equidistance from both the walls). (c) Slip velocity, drop deformation
- 5 (inset) and (d) migration velocity a viscous drop in a viscoelastic fluid for three grid resolutions in
- two reference frames for Ca=0.2, De=0.5,  $\lambda_u=1.0$  and initial position  $h_i/a=1.35$ .
- Figure 2. Lateral velocity, deformation and orientation angle for Ca = 1.5,  $\lambda_{\mu} = 10$ , and  $h_i/a = 1.5$
- 8 are compared with BEM simulations of Uijttewaaal and Nijhof (UN). Dotted curves in color blue
- 9 (our simulation) and red (BEM) are computed with initially fully developed shear for the viscous
- case (De = 0). The other two curves are with impulsively started flow for De = 0 (solid) and De = 0
- 11 0.25 (dash).

- Figure 3. Drop migration for varying De for Ca = 0.2,  $\lambda_{\mu} = 10$  and  $h_i / a = 1.5$ : (a) Drop height with
- time (Inset shows the lateral velocity), (b) net viscoelastic force on the drop in the y-direction, (c)
- deformation and inclination angle, and (d) slip velocity.
- 16 Figure 4. Lateral migration velocity as a function of the distance from the wall for Newtonian and
- viscoelastic cases for Ca = 0.2,  $\lambda_u = 10$  and varying De.
- Figure 5. (a) Non-dimensional height vs. time for Ca = 0.2, De = 0.75, and  $h_i/a = 1.5$ . The inset
- shows the time variation of lateral velocity. (b) Time evolution of slip velocity for the same pa-
- 20 rameters.
- Figure 6. Quasi-steady migration velocity as a function of viscosity ratio, at two different Deborah
- numbers and h/a (legends are same as in the inset) for Ca = 0.2. Inset shows the same scaled by
- 23  $(a/h)^2$ .
- 24 Figure 7. Evolution of the non-dimensional drop height for different capillary and Deborah num-
- bers and  $\lambda_u = 10$ .

- Figure 8. (a) Quasi-steady velocities plotted vs. drop height for Ca = 0.05 and De = 0.75 for dif-
- 2 ferent viscosity ratios. (b) Shapes of drops (horizontal position is arbitrary) migrating towards the
- wall (black line) at successive time instants for De = 0.75, Ca = 0.05,  $h_i/a = 1.5$ ,  $\lambda_u = 10$  (top) and
- 4 De = 0.75, Ca = 0.2,  $h_i/a = 1.5$ ,  $\lambda_u = 20$  (bottom).
- Figure 9. Lateral migration velocities plotted for  $\lambda_{\mu} = 10$  and at instantaneous height of 1.4a to
- 6 show Capillary variation of lateral velocities for different Deborah numbers. Inset shows the lateral
- 7 velocities divided by *Ca*.

- 9 **Figure 10**. Phase diagrams for the direction of drop migration: (a) In  $\lambda_{\mu}$  -Ca space for De = 0.75
- and  $h_i/a = 1.5$ . (b) In De-Ca space for  $\lambda_{\mu} = 10$ ,  $h_i/a = 1.5$ . Drops below the green lines migrate away
- from the wall and those above migrate towards the wall. The color contour describes the migration
- 12 velocity.